Macromolecules
ARTICLE

Macromolecules **2009**, *42*, 6917–6926 **6917**
DOI: 10.1021/ma9013127

Design and Synthesis of Dual Thermoresponsive and Antifouling Hybrid Polymer/Gold Nanoparticles

Cyrille Boyer,[†] Michael R. Whittaker,[†] Mario Luzon,[‡] and Thomas P. Davis*,[†]

[†]*Centre for Advanced Macromolecular Design (CAMD), School of Chemical Sciences and Engineering, The University of New South Wales, Sydney, NSW 2052, Australia, and* [‡]*Instituto de Ciencia y Tecnología de Polímeros, C.SIC; C/Juan de la Cierva 3, 28006 Madrid, Spain*

Received June 18, 2009

ABSTRACT: A series of thermosensitive copoly(oligoethylene oxide) acrylates with narrow polydispersities were prepared by the copolymerization of oligo(ethylene oxide) acrylate and di(ethylene oxide) ethyl ether acrylate using reversible addition−fragmentation chain transfer polymerization (RAFT). These copolymers exhibit tunable LCST behavior over the range of 15−90 °C dependent on their monomer compositions. Subsequently, these copolymers were grafted onto gold nanoparticle (GNP) surfaces yielding thermosensitive gold nanoparticles. The thermoresponsive properties of these hybrid GNPs/poly(OEG-A-*co*-DEG-A) nanoparticles were evaluated in solution using dynamic light scattering and UV−vis spectroscopy. In addition, the susceptibility of these GNPs to protein fouling was assessed by a Bradford's assay and found to be significantly reduced by the copolymer stabilizing layer. We also demonstrate, in a unique one-pot assembly process, the synthesis of a hybrid nanoparticle that shows dual temperature responsiveness. These hybrid nanoparticles open new applications in biotechnology and medicine.

Introduction

"Thermoresponsive" and functional gold nanoparticles[1] (GNP) have received considerable interest for applications in a diverse range of areas embracing biotechnology,[2−15] nanotechnology,[16−19] and catalysis.[20−24] Their unique optical and scattering properties combined with a pre-engineered ability to respond predictably to their environment in solution confers interesting attributes for use as targeted vectors for drug/gene delivery[12,25−28] and contrast agents.[2,5,29−32] To impart desirable responsive properties and to improve their stability in solution, an appropriate functional/responsive polymer layer can be grafted to these GNPs using either the grafting "from"[33−38] or "to"[39−41] approaches. The "pros" and "cons" of both these methods have been widely discussed.[42,43] Recent work has shown that well-defined polymers synthesized via RAFT polymerization can bind inherently to gold, making the "grafting to" method particularly attractive and versatile. This was demonstrated for the first time by McCormick, Lowe, and Sumerlin et al.[39,44−47] and later by other teams.[48−51] These RAFT-derived polymers have inherent gold binding abilities originating from the RAFT end groups (typically di- and trithio compounds) (Scheme 1).[52−55] In addition, RAFT end-group functionality can be transformed easily to the established gold binding functionality of thiol (Scheme 1).[56−59]

In such applications as targeted drug/gene delivery and imaging agents, these nanoparticles must not only show targeted or responsive behavior, but it is also important that they evade the reticuloendothiel system (RES).[60] It is this system that is responsible for the rapid clearance of these particles from the body. In the above applications the blood circulation time is critical for their success. However, the incorporation of a thermoresponsive polymer layer often enhances protein absorption and specific biomolecular tagging processes, leading to faster clearance times of nanoparticles from the body. PEGylation has been a common strategy employed to increase the blood residence time of not only nanoparticles[61−64] but also a diverse range of therapeutic molecules.[65−68] These PEGylation processes, while providing "stealth" characteristics, fail to impart any thermoresponsive behavior to the nanoparticles and hence limit their application in these newer technologies.

Previously, several authors have coated GNPs with thermosensitive polymers,[69−73] thereby conferring new properties. Conventionally, the favored thermosensitive polymer has been poly(*N*-isopropylacrylamide) (PNIPAAm).[69−73] PNIPAAm has a lower critical solution temperature (LCST) of 31−32 °C in water.[74−76] However, the grafting of PNIPAAm on GNPs suffers from some limitations: (i) PNIPAAm presents only one fixed LCST; (ii) the presence of amide groups on the GNP surface can induce protein adsorption leading to fast clearance rates from the body. To improve the potential of PNIPAAm, different authors have attempted to tune the thermoresponsive behavior of PNIPAAm by copolymerization with a pH-sensitive monomer[77−79] or by the addition of hydrophilic/hydrophobic monomers such acrylamide[80] during the polymerization. In addition, the use of block copolymers of PNIPAAm with PEG has been explored, with the block lengths used as a design tool for tuning the LCST behavior.[81,82] Moreover, antifouling properties can be controlled using the LCST of the PNIPAAm block.[83,84]

Recently, a new class of polymers combining temperature responsiveness and antifouling/stealth behavior has been reported. These brushlike macromolecules, based on copolymers of di(ethylene glycol) methyl ether methacrylate (DEG-MA) and oligoethylene glycol methacrylate (OEG-MA), are analogues of linear PEG.[85−87] These copolymers present tunable thermoresponsive behavior and additional properties such as biocompatibility, protein adsorption resistance, and stealthlike behavior (analogous with linear PEG).[64,88]

Herein, we report the RAFT synthesis of thermosensitive PEG-based polymers using acrylic monomers, i.e., di(ethylene

*Corresponding author. E-mail: t.davis@unsw.edu.au.

Published on Web 07/10/2009

Scheme 1. Schematic Representation of the Interaction Gold−Thiol Polymers and Gold−Trithiocarbonate Polymers

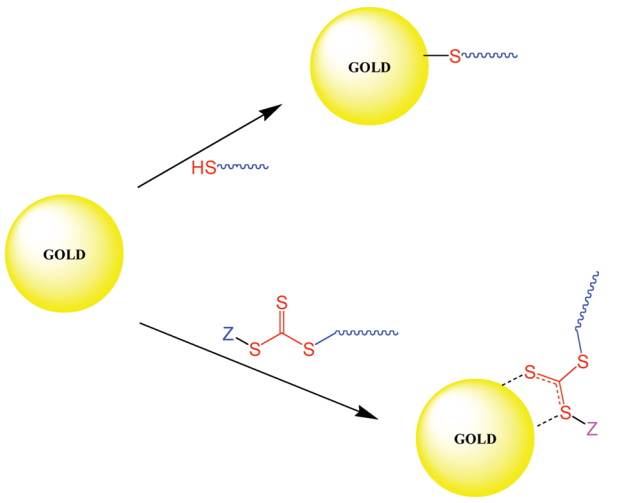

glycol) ethyl ether acrylate (DEG-A) and oligoethylene glycol acrylate (OEG-A). These copolymers, obtained using RAFT polymerization, present tunable LCSTs similar to their methacrylic analogues. Their use in the "grafting-to" procedure for GNP modification is described for the formation of GNP/polymer hybrid nanoparticles. Copolymers of poly(OEG-acrylate) and di(ethylene glycol) ethyl ether acrylate were prepared having LCST values ranging from 15 to 90 °C. These copolymers were grafted onto GNP surfaces, yielding thermosensitive gold nanoparticles. The hybrid GNPs/copolymer nanoparticles possess similar temperature responsive properties to established gold/PNIPAAm particles but more importantly have additional properties that make then more suitable for use in bioapplications. The presence of a poly(OEG-A-*co*-DEG-A) layer confers an antifouling surface on the GNPs, resistant to protein adsorption. To our knowledge, it is the first time GNPs have been coated with a polymer coating imbuing thermoresponsive behavior, antifouling, and potential stealth properties.

Experimental Part

Materials. Oligoethylene glycol acrylate (OEG-A) (**1**, number-average molecular weight $M_n = 450$ g/mol, PDI = 1.02) and di(ethylene glycol) ethyl ether acrylate (**2**) were purified via an alumina column to remove the inhibitor prior to use. *N*-Isopropylacrylamide (NIPAAm) (Aldrich, 99%) was crystallized twice from hexane prior to use. 2,2′-Azobis(isobutyronitrile) (AIBN) was purchased from Wako Chemicals and was crystallized twice from methanol prior to use. Hydrogenotetrachloroaurate(III) hydrate ($HAuCl_4$, 99.9%, Aldrich), trisodium citrate dehydrate (99%, Aldrich), bovine serum albumin (BSA, 99%, Aldrich), and pyrene (99.9%, Fluka) were used as received. Deionized water used for these experiments were purified by MILIQ system with a resistivity of 17.9 mΩ/cm.

Analytical Techniques. *Size Exclusion Chromatography (SEC).* Aqueous size exclusion chromatography (SEC) was implemented using a Shimadzu modular system comprising a DGU-12A solvent degasser, a LC-10AT pump, a CTO-10 A column oven, a RID-10A refractive index detector, and a SPD-10A Shimadzu UV−vis detector (flow rate: 1 mL/min). The column was equipped with a PL 5.0 mm bead-size guard column (50×7.8 mm^2) followed by three PL aquagel-OH columns (50, 40, 30; 8 μm). Calibration was performed with PEO standards ranging from 500 to 500 000 g/mol. SEC analyses of the polymers were also performed in *N*,*N*-dimethylacetamide [DMAc; 0.03% w/v LiBr, 0.05% 2,6-dibutyl-4-methylphenol (BHT)] at 50 °C (flow rate = 1 mL/min) using a Shimadzu modular system comprising an SIL-10AD autoinjector and a PL 5.0 mm bead-size guard column (50 × 7.8 mm) followed by four linear PL (Styragel) columns (10^5, 10^4, 10^3, and 500 Å) and an RID-10A differential refractive index detector and in tetrahydrofuran (THF) at 40 °C (flow rate = 1 mL/min) using a Shimadzu modular system comprising an SIL-10AD autoinjector and a PL 5.0 mm bead-size guard column (50 × 7.8 mm) followed by four linear PL (Styragel) columns (10^5, 10^4, 10^3, and 100 Å). Calibration was achieved with commercial polystyrene standards ranging from 500 to 10^6 g/mol.

UV−vis Spectroscopy. UV−vis spectra were recorded using a CARY 300 spectrophotometer (Bruker) equipped with a temperature controller.

NMR Spectroscopy. ^{1}H and ^{13}C NMR spectra were recorded on a Bruker ACF300 (300 MHz) or ACF500 (500 MHz) spectrometer, with D_2O or $CDCl_3$ used as solvents. NIPAAm monomer conversion was determined by comparing the vinyl proton signal ($\delta \sim 5.4-6.3$, 3H/mol NIPAAm monomer) to the total isopropyl methylene signal ($\delta \sim 3.6-3.85$ 1H/mol NIPAAm).

Infrared Spectroscopy. FT-IR spectra were obtained using a Bruker Spectrum BX FT-IR system using diffuse reflectance sampling accessories and a resolution of 2 cm^{-1}. Each sample was analyzed using 128 scans.

Dynamic Light Scattering (DLS) and Zeta Potential. Dynamic light scattering studies of the GNPs at 5 mg/mL in an aqueous were conducted using a Malvern Instruments Zetasizer Nano ZS instrument equipped with a 4 mV He−Ne laser operating at $\lambda = 633$ nm, an avalanche photodiode detector with high quantum efficiency, and an ALV/LSE-5003 multiple tau digital correlator electronics system.

Microscopies. TEM and AFM. The sizes and morphologies of the nanoparticles were observed using a transmission electron microscopy JEOL1400 TEM at an accelerating voltage of 100 kV. The particles were dispersed in water (1 mg/mL) and deposited onto 200 mesh, holey film, copper grid (ProSciTech). For the preparation of samples above the LCST, the solution was heated to $T > T^{LCST}$, and at the same time, a copper grid was also equilibrated at this temperature. A few drops of the heated nanoparticles solution were then placed on the copper grid and dried in the oven ($T > T^{LCST}$).

For atomic force microscopy (AFM), GNP solutions (200 μL) were deposited on a mica surface and dried at temperatures below or above the LCST. The sample was characterized by AFM (Digital Instruments 3000 AFM) in tapping mode.

Methods. *LCST Measurement.* The lower critical solution temperature, LCST, was determined by a UV−vis spectrophotometer at 500 nm. The polymer concentrations were 0.2 mg/mL (0.2 wt %) in water with a heating rate of 1 °C/min. The temperature at which 10% of the maximum absorbance of the solution was observed was defined as the LCST.

Determination of Particle Size. GNPs (or GNPs/polymer) solutions were prepared in distilled water with GNP concentrations of 5 mg/mL. The solution was filtered trough Millipore nylon filters (pore size 0.45 μm) to eliminate dust and large contaminants. The size measurements were carried out in a quartz cuvette, and the temperature was allowed to equilibrate for 5 min. For the determination of size vs temperature the heating rate was 1 °C/min.

Syntheses. *Synthesis of Gold Nanoparticles.* Citrate-stabilized gold nanoparticles (20 nm) were prepared using published procedures.[89] Briefly, all glassware was first washed with an aqua regia solution (25 vol % nitric acid and 75 vol % concentrated hydrochloric acid), then rinsed with Milli-Q water several times, and dried. Milli-Q water (100 mL) and 1% solution trisodium citrtate dehydrate (5 mL, 1.053 g of trisodium citrtate) were mixed. The solution was heated up to boiling point with vigorous stirring, and then hydrogenotetrachloroaurate(III) hydrate stock solution (0.01 M) (2.54 mL) was introduced rapidly using a syringe. The solution was boiled for a further 30 min with vigorous stirring.

A progressive change of color was observed from yellow to wine red. The solution was cooled down and stored in a fridge at 5 °C until required. The particles were characterized by TEM and DLS.

Synthesis of RAFT Agents. The syntheses of 3-(benzylsulfanylthiocarbonylsulfanyl)propionic acid (**3**, BSPA) is described elsewhere.[59]

RAFT Polymerizations. *RAFT Polymerization of NIPAAm in the Presence of 3-(Benzylsulfanylthiocarbonylsulfanyl)propionic Acid (BSPA)*. An example of polymerization of NIPAAm is given for $[NIPAAm]_0/[CTA]_0/[AIBN]_0 = 250/1/0.2$. NIPAAm (1.13 g, 0.01 mol), 3-(benzylsulfanylthiocarbonylsulfanyl)propionic acid (10 mg, 3.64×10^{-5} mol), AIBN (1.2 mg. 7.3×10^{-6} mol), and acetonitrile (10 mL) were mixed. The solution was cooled in an ice bath and purged with nitrogen for 30 min before heating to 65 °C. After 5 h, the solution was partially evaporated under vacuum, and the polymer was precipitated in cold diethyl ether (at 0 °C). The precipitation was repeated twice more to remove any unreacted monomer or residual RAFT agent. The product was dried in vacuo to yield a yellow powder.

RAFT Polymerization of Di(ethylene glycol) Ethyl Ether (DEG-A) in the Presence of 3-(Benzylsulfanylthiocarbonylsulfanyl)propionic Acid (BSPA). An example of polymerization of DEG-A is given for $[DEG\text{-}A]_0/[CTA]_0/[AIBN]_0 = 150.0/1.0/0.2$. DEG-A (1.88 g, 0.01 mol), 3-(benzylsulfanylthiocarbonylsulfanyl) propionic acid (30 mg, 3.64×10^{-5} mol), AIBN (2.0 mg. 1.22×10^{-5} mol), and acetonitrile (10 mL) were mixed. The solution was cooled in an ice bath and purged with nitrogen for 30 min before heating to 60 °C. After 5 h, the solution was partially evaporated under vacuum, and the polymer was precipitated in cold diethyl ether (at 0 °C), yielding a viscous yellow product. The precipitation was repeated twice more to remove any unreacted monomer or residual RAFT agent. The product was dried in vacuo to yield a yellow viscous product.

A similar process was repeated for all the polymerizations with OEG-A and the copolymerization with OEG-A and DEG-A.

Grafting of Polymer "to" GNPs. A stirred GNP solution (10 mL of 1 mg/mL previously obtained) was placed in an ice bath under for 30 min. Cooled polymer solution (1 mL concentration: 30 mg/L) was added to the GNP solution, followed by stirring for 30 min. Then, the GNPs were purified by centrifugation at 20 000 rpm for 30 min at 5 °C followed by resuspension in cooled water. This process was repeated three times. GNPs/polymer nanoparticles were stored in solution (10 mg/mL) or freeze-dried. After freeze-drying the hybrid GNP/polymer nanoparticles could be redispersed easily in water (in contrast to GNPs with no polymer coating).

Protein Adsorption. GNP/polymer nanoparticles (1.0 mg/mL) prepared above were suspended in aqueous solution with bovine serum albumin (BSA) at an initial concentration of 1 mg/mL (pH = 6.5). The samples were then shaken at room temperature for 3 h to reach adsorption equilibrium. GNPs were removed by centrifugation, and the supernatant was analyzed for BSA. The supernatant BSA concentrations were determined via the Bradford method[90] using a UV−vis spectrometer (Varian Cary 300 scan). An aliquot of the supernatant (10 μL) was then added to Bradford's reactant (3 mL) and mixed for 2 min at room temperature (the solution becomes blue). The concentration of BSA was measured by absorption at 595 nm. The test was repeated three times for each sample. The average of the replicate measurements was taken to determine the BSA concentration at equilibrium. The amount of BSA adsorbed was calculated by difference from a reference solution (solution treated using the same method but without gold nanoparticles).

$$\%BSA_{adsor} = 100 - (([BSA]_{eq}/[BSA]_0) \times 100)$$

where $[BSA]_0$ and $[BSA]_{eq}$ correspond to BSA concentrations measured by Bradford's assay without GNPs and BSA concentrations in the presence of GNPs at equilibrium, respectively.

Fluorescence Measurements. GNPs/[poly(DEG-A)/poly(OEG-A-*co*-DEG-A) = 50/50 wt %] (5 mL, 1 mg/mL) were mixed with pyrene/acetone solution (50 μL) (10^{-4} M) overnight at 5 °C. GNP solution (2 mL) was charged to a 1.0 cm square quartz cell. The solution was carefully heated from 5 to 40 °C (at a heating rate of 0.5 °C/min) under analysis using a fluorescence spectrophotometer (Varian fluorescence spectrophotometer) at an excitation wavelength of 335 nm.

Results and Discussion

The synthesis of different poly(OEG-A-*co*-DEG-A) compositions was achieved by RAFT polymerization using 3-(benzylsulfanylthiocarbonylsulfanyl)propionic acid (BSPA, **3**) as the RAFT agent and AIBN as the initiator (Scheme 2). A summary of the different copolymers obtained and their characteristics is given in Table 1. Copolymer compositions were determined via ^{1}H NMR using the characteristic signal at 1.1 ppm from CH_3 of DEG-A and at 3.6 ppm from $-OCH_2-$ of the OEG chain (Figure S1 in the Supporting Information). The feed ratios and the compositions of the copolymers were proximate, indicating that these two monomers have similar reactivity in the RAFT-mediated copolymerization reaction. Moreover, the good correlation between the targeted and experimental molecular weights and the attainment of narrow polydispersities (PDIs below 1.2) for all the copolymers indicates effective RAFT control.

The maintenance of the RAFT end groups (after purification), an essential factor for the subsequent modification of the GNPs, was confirmed by UV−vis spectroscopy using the characteristic absorbance peak at 305 nm of the trithiocarbonate end group and the following equation: $f^{RAFT} = 100 \times [Abs^{305\,nm}/\varepsilon^{RAFT}]/[polymer]_0$, where $Abs^{305\,nm}$, ε^{RAFT}, and $[polymer]_0$ correspond to the absorbance of RAFT agent, extinction coefficient, and polymer concentration, respectively. All the characterized copolymers had a RAFT end-group functionality greater than 85%.

Scheme 2. Copolymerization of Oligo(ethylene glycol) Acrylate (1) and Di(ethylene glycol) Acrylate (2) Using 3-(Benzylsulfanylthiocarbonylsulfanyl)propionic Acid (BSPA, 3)

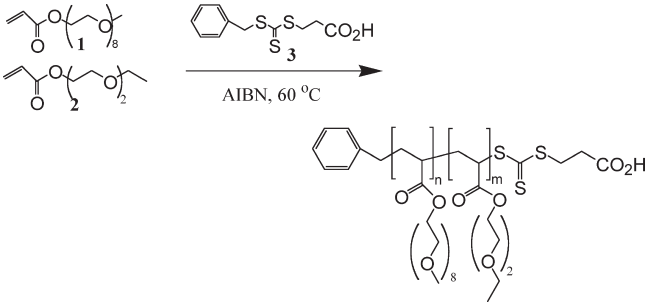

Table 1. Summary of Polymers and Copolymers Used in This Study

	feed ratio (mol %)		composition[a] (mol %)				
entry	OEG-A	DEG-A	OEG-A	DEG-A	M_n[b] (g/mol)	PDI[b]	T(LCST)[c] (°C)
1	0	100	0	100	21 500	1.23	15
2	5	95	6	94	22 200	1.26	22
3	10	90	10	90	20 300	1.22	33
4	15	85	16	84	18 600	1.24	45
5	20	80	20	80	22 300	1.22	50
6	25	75	26	74	21 400	1.25	58
7	30	70	29	61	18 500	1.24	65
8	50	50	45	55	20 500	1.26	72
9	100	0	0	100	21 200	1.24	92

[a] Determined by ^{1}H NMR. [b] Assessed by DMAc GPC (poly(styrene) calibration). [c] LCST assessed by turbidity measurement at 500 nm assessed by UV−vis measurement.

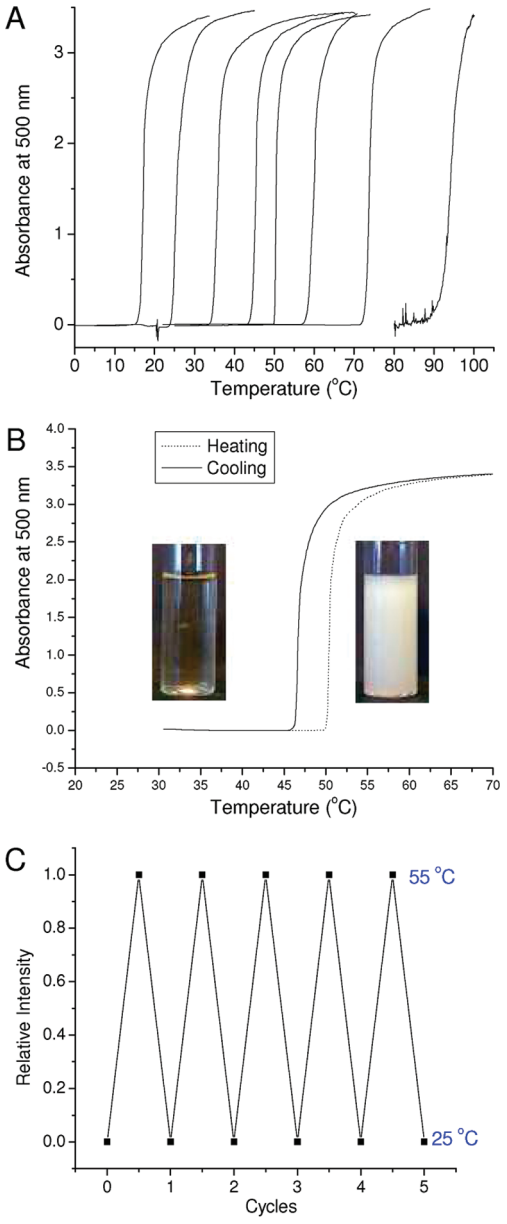

Figure 1. Thermal properties for the copolymers obtained by RAFT polymerizations. (A) UV−vis turbidity measurement of copoly[(OEG-A)-*co*-(DEG-A)] (left to right: entry 1 to 9 of Table 1) for the heating cycle. (B) UV−vis turbidity measurement of copoly[(OEG-A)-*co*-(DEG-A)] (run 4 of Table 1) for the heating and cooling cycle. Inset: picture of solution below and above the LCST. (C) Relative intensity of copoly[(OEG-A)-*co*-(DEG-A)] for several cycles.

The water LCST behavior of these different copolymers (1 mg/mL) was determined by turbidity measurements (at λ = 500 nm) as a function of temperature. Poly(DEG-A) was found to have a LCST of 15 °C, while poly(OEG-A) has an LCST close to 90 °C (Figure 1A). These LCST values are consistent with previously published work.[86] Increasing the concentration of the DEG-A monomer in the copolymer chain decreases the LCST and allows the synthesis of copolymers with LCST values ranging from 15 to 90 °C (Table 1). A small hysteresis (~5 °C) effect was observed between the heating and cooling cycles (Figure 1B). When the heating−cooling cycles were repeated several times, there was no significant shift in either the LCST or the measured absorbance during these cycles (Figure 1C). It is noteworthy that the polymer chain-length control exerted by RAFT polymerization results in an improved thermosensitivity response of these copolymers when compared to chains synthesized by conventional free radical polymerization. Indeed, the presence of a broad distribution of chain lengths in the case of free radical polymerization results in a broader LCST transition when heated and a larger hysteresis effect on cooling. This result is in accord with the ATRP results given by Lutz and co-worker[86] for similar copolymers.

Highly uniform gold nanoparticles (GNP) were synthesized via the established citrate reduction method[89] (reduction of $HAuCl_4$ by boiling with sodium citrate) to yield spherical gold nanoparicles with a diameter close to 20 nm as observed by transmittance electronic microscope (TEM) and by dynamic light scattering (DLS) (see Figure S2 in the Supporting Information). GNP size can be tuned from 10 to 150 nm using our approach; smaller sizes can obtained using other techniques.[91] In the present case, we selected a size around 20 nm as model (commonly used in the literature),[92−94] as these GNPs can be purified easily using centrifugation techniques. Indeed, smaller GNPs can be difficult to purify by centrifugation, while bigger GNPs typically show broader size distributions. However, the approach described in this paper for the coating of 20 nm nanoparticles could be applied easily to both larger and smaller GNP sizes.

RAFT functionalized copoly(DEG-*co*-OEG) in aqueous solution was mixed with the GNPs, and the strong affinity of the trithiocarbonate functionality for the gold surface resulted in the assembly of polymers onto the gold surface.[54] After polymer attachment, the solution undergoes a slight color change (Figure S2 in the Supporting Information), accompanied by a blue shift (typically, 5−10 nm) of the characteristic plasmon resonance absorption peak at 525 nm. Extraneous nongrafted copolymer chains were removed by repeated washing/centrifugation cycles with ultrapure water. The purified gold/polymer hybrid nanoparticles were finally redispersed in water. It was found that the attached polymer shell was imperative for GNP redispersal in water after centrifugation. DLS measurements confirmed that coating GNPs with copoly(DEG-*co*-PEG) results in an increase in the hydrodynamic diameter of the nanoparticles (see Figure S2 in the Supporting Information). In addition, TEM images of the polymer-coated GNPs show well-dispersed particles with minimal aggregation (Figure 2). Further TEM characterization using phosphotungsten acid as a negative stain confirmed the presence of a grafted polymer layer as shown by contrasting white halos around the GNPs (inset of picture A, Figure 2). AFM measurements confirmed the presence of hybrid GNPs with sizes ranging from 20 to 30 nm. The phase contrast image (inset of picture F, Figure 2) of the same hybrid particles confirms the presence of a soft shell (polymer) around a hard gold core.

The zeta potentials of the GNPs both before and after grafting were measured, recording an increase from ~−40 to ~0 mV (±5 mV). This result is consistent with an exchange of the negative citrate ions on the GNP surface (originating from the GNP synthetic method) with the uncharged polymer stabilizing layer.

The presence of a grafted copolymer layer on the GNPs was accrued using ATR (Figure 3) and X-ray photoelectron spectroscopy (XPS) (Figure 4). As expected, the ATR of the hybrid GNPs reveal characteristic PEG absorption signals: the C−O ether bond at 1480 cm^{-1} and the C═O carbonyl bond at 1730 cm^{-1}. In addition, as the copolymer composition of the polymer shell changes (with increased DEG), a concomitant increase in the absorption of the carbonyl bond, relative to the ether bond, is observed. XPS measurements indicate different elemental signals attributable to the carbon, oxygen, and sulfur atoms at the surface of the hybrid GNPs. High-resolution XPS confirms the presence of C(1s) from the C−O ether bond (at 286.45 eV)[95] and the presence of an intense signal associated with oxygen (1s) at 532.38 eV.[96] In addition, XPS detected sulfur bonds S(2p) at 162.0 and at 163.4 eV originating from the

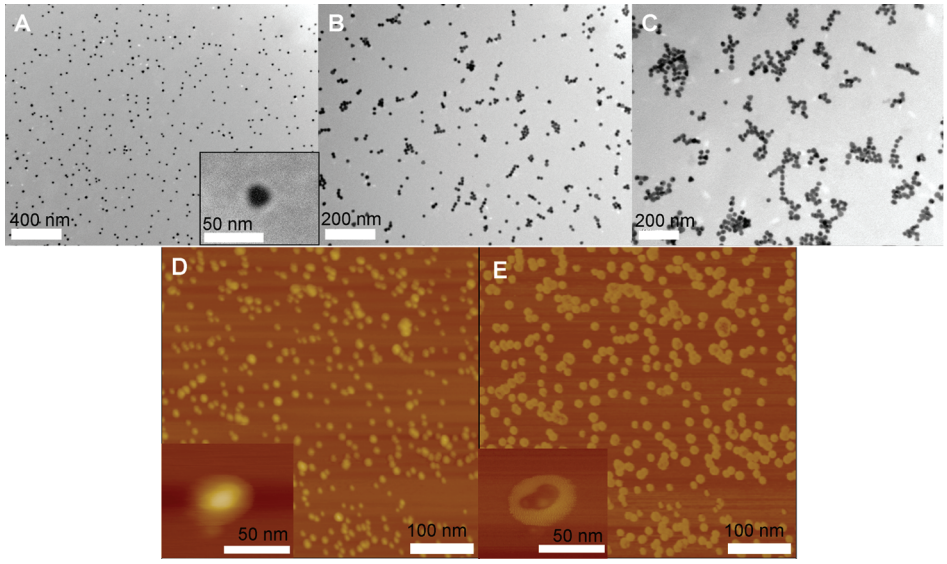

Figure 2. TEM and AFM pictures of GNPs/poly(DEG-*co*-OEG-A) (entry 3). (A) At 25 °C; inset: particle with phosphotungsten acid as contrast agent. (B) At 30 °C and (C) at 35 °C. (D, E) AFM pictures of GNPs/poly(DEG-*co*-OEG-A): (D) contact and (E) phase.

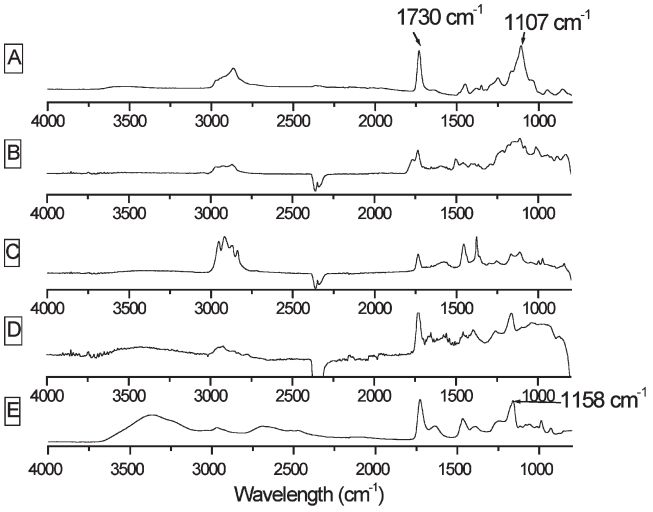

Figure 3. ATR analyses purified GNPs/poly(OEG-*co*-DEG-A): (A) GNPs/poly(OEG-A), (B) GNPs/poly(OEG-*co*-DEG-A) [entry 2 of Table 1]; (C) GNPs/poly(OEG-*co*-DEG-A) [entry 6 of Table 1]; (D) GNPs/poly(OEG-*co*-DEG-A) [entry 8 of Table 1]; (E) GNPs/poly-(OEG-*co*-DEG-A) [entry 9 of Table 1].

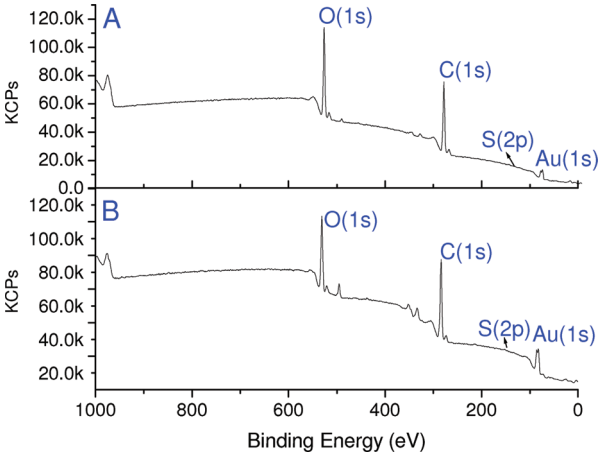

Figure 4. XPS analyses: (A) GNPs/poly(OEG-*co*-DEG-A) [entry 6 of Table 1]; (B) GNPs/poly(OEG-*co*-DEG-A) [entry 2 of Table 1].

gold−sulfur bond. Recently, Theato and co-worker[55] reported surface plasma resonance (SPR) experiments confirming that the dithioester moiety (the RAFT end group here) can bind directly with gold surfaces. However, the gold−dithioester interaction has been found to be less stable than gold−thiol interactions.[53,55]

The thermoresponsive character of the gold/polymer hybrid nanoparticles in aqueous solutions was demonstrated by non-isothermal turbidity measurements. On heating to the vicinity of the LCST transitions, the GNP aqueous solution changes color from red to purple (a shift of the wavelength from 520 to 600 nm), as shown in Figure 5. The color of GNPs is known to depend on both their dimensions and their environment. On GNP aggregation, the characteristic GNP plasmon resonance of 520 nm (red solution) shifts toward longer wavelengths (blue solution) characteristic of an increased electronic dipole−dipole interaction among near-neighbor GNPs. In addition, as the absorbance wavelength shifts, there is also a decrease in the measured absorbance intensities. Maintaining the GNP solution above the LCST for several hours results in a purple precipitate; however, this can be redispersed rapidly by cooling the mixture below the LCST with gentle shaking. UV−vis spectroscopy measurements were used to confirm the reversible nature of the LCST transition. The aggregates formed above the LCST were characterized using DLS measurements, confirming the presence of aggregates with sizes of 200 nm, as shown in Figure 6. TEM was also applied to characterize the aggregates, revealing the formation of GNP chains consisting of 8−12 nanoparticles (pictures B and C, Figure 2). On cooling, below the LCST, the aggregates observed by both DLS and TEM disappeared (Figure 6C). However, the temperature of dissociation and redispersion of these aggregates was always found to be slightly lower (∼5−8 °C) than the temperature observed for their aggregation. DLS data show that the particles returned to their original sizes (measured below the LCST) after a complete heating−cooling cycle. No change in their spectroscopic properties (such as λ_{max} and average size) could be detected after several heating−cooling cycles (Figure 6D).

Attached PEG copolymers are known to imbue favorable characteristics to metal nanoparticles,[31,97] including antifouling and stealth characteristics, as demonstrated by both in vitro and in vivo testing.[11,31,98−105] To investigate these properties further, the nanoparticles prepared in this study were subjected to

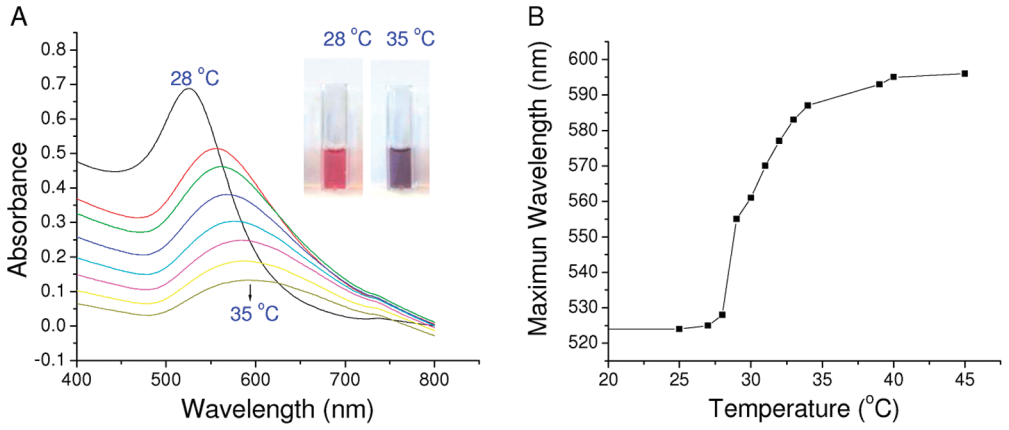

Figure 5. (A) UV−vis spectra of GNPs/poly(OEG-A-*co*-DEG-A) (entry 3 of Table 1) versus temperature. Each spectrum was taken after increasing of 1 °C (from 28 to 35 °C). Inset: picture of gold/poly(OEG-A-*co*-DEG-A) dispersed in water at 25 and 35 °C, respectively. (B) Evolution of maximum wavelength versus temperature.

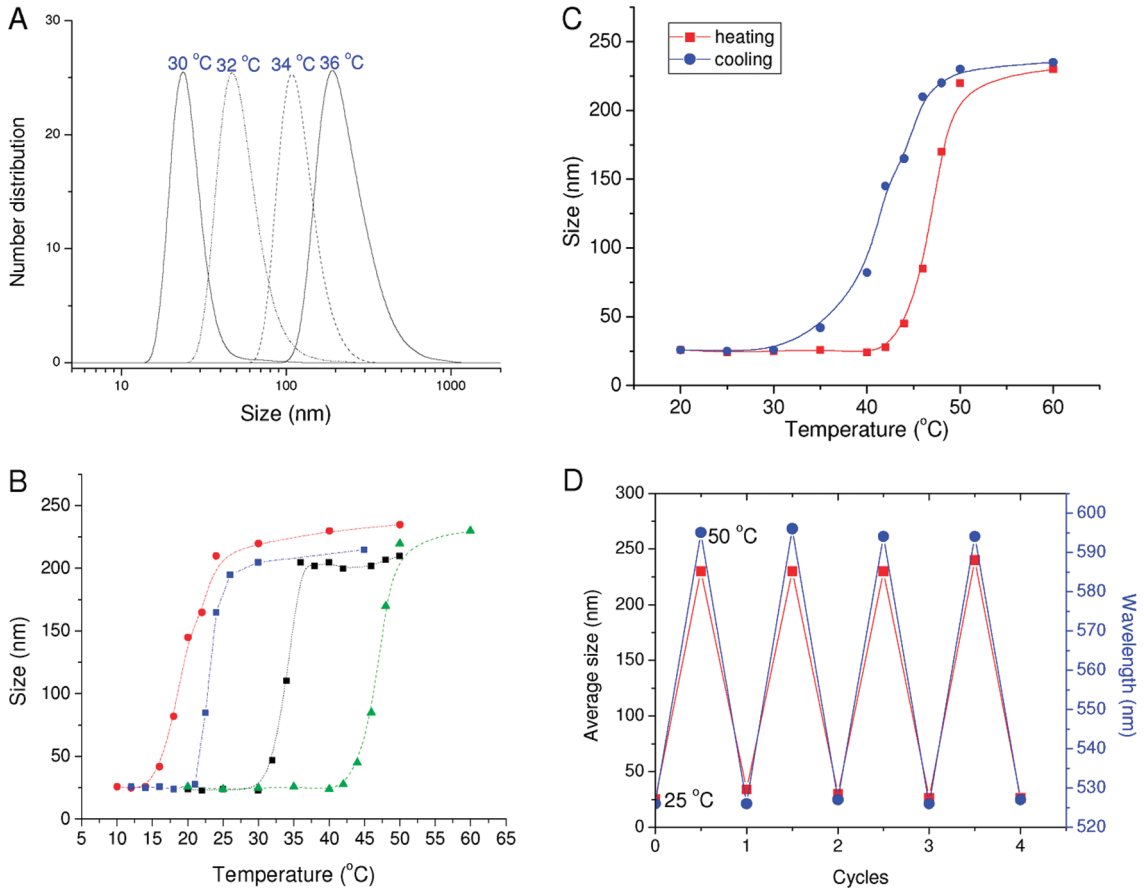

Figure 6. Number distribution versus size (nm) for GNPs coated with poly(DEG-*co*-OEG-A): (A) Evolution of size at different temperatures for poly(DEG-*co*-OEG-A): entry 3 of Table 1. (B) Evolution of average size (determined from the number distributions) versus temperature for four different GNPs/poly(DEG-*co*-OEG-A) (red curve: entry 1 of Table 1; blue curve: entry 2 of Table 1; black curve: entry 3 of Table 1; green curve: entry 4 of Table 1). (C) Evolution of average size (determined from the number distributions) versus temperature for GNPs/poly(DEG-*co*-OEG-A) (entry 4 of Table 1) (heating and cooling cycle). (D) Variation of the average sizes and λ_{max} (assessed by UV−vis spectroscopy) for different cooling/heating cycles of GNPs/poly(DEG-*co*-OEG-A) (entry 4 of Table 1).

Bradford assays, using BSA as a model protein. The Bradford assay[90] evaluates the amount of unbound BSA after 3 h of incubation with the GNP dispersion. After incubation, the GNPs were removed from solution by centrifugation, and the supernatant was analyzed for the presence of "free" BSA. Two control assays were also conducted to afford comparisons with "naked" GNPs (stabilized by citrate) and GNPs stabilized with PNIPAAm. The results from the Bradford assays, showing the proportion of BSA adsorbed onto each of the nanoparticles, are given in Figure 7. In the presence of a poly(OEG-A-*co*-DEG-A) stabilizing layer below the LCST, less than 0.10 (±0.07) mg/m^2 (9×10^{14} molecules/m^2) of BSA was adsorbed. This low adsorption yield is close to the experimental error and can be interpreted as effectively zero adsorption. When the level of DEG-A in the copolymer is increased, the BSA adsorption (below the LCST) slightly increased (from 0.10 to 0.15 (±0.07) mg/m^2) (Figure 7). A hypothesis can be tendered that the length of ethylene glycol is insufficient to confer perfect antifouling

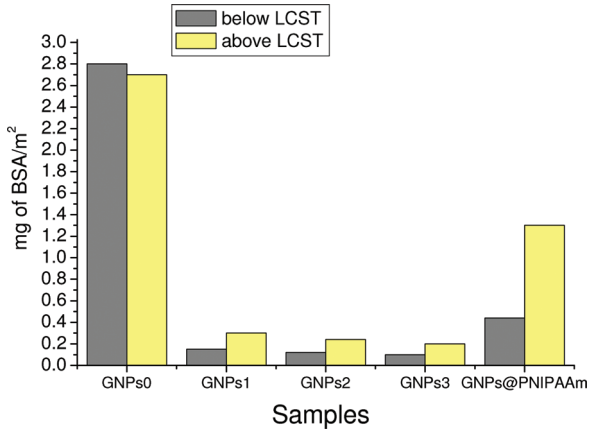

Figure 7. BSA absorption on different GNPs: "naked" GNPs (0), GNPs (1): GNPs/poly(OEG-*co*-DEG-A) [entry 2 of Table 1]; GNPs (2): GNPs/poly(OEG-*co*-DEG-A) [entry 3 of Table 1]; GNPs (3): GNPs/poly(OEG-*co*-DEG-A) [entry 4 of Table 1]; GNPs/PNIPAAm, M_n = 20 000 g/mol, PDI = 1.08. Note: BSA absorbed calculated by $100 \times (1 - (Ab_{GNP}^{595\,nm}/Ab_{(0)}^{595\,nm}))$, where $Ab_{GNP}^{595\,nm}$ and $Ab_{(0)}^{595\,nm}$ correspond to absorbance of Bradford reactant after incubation with and without GNPs, respectively.

behavior as the number of ethylene glycol units is an important parameter for controlling the adsorption of protein on surfaces.[106] In contrast, 0.44 mg of BSA /m^2 (±0.10) in solution was adsorbed onto nanoparticles stabilized with PNIPAAm at 25 °C; a result strongly favoring the use of these thermoresponsive PEGs where GNPs are used in bioapplications. Finally, in the absence of any polymer coating, 2.8 mg/m^2 (or 2.5 × 10^{16} BSA/m^2) was adsorbed from solution onto the gold surface, consistent with strong charge interactions between the citrate stabilizing groups and the protein. This measured adsorption corresponds (assuming BSA dimensions of 5.5 × 5.5 × 9.0 nm) to the formation of a BSA monolayer on the GNPs obtained for an end-on binding mechanism (theoretical values are 3.3 and 2.0 mg/m^2 for an end-on and a side binding, respectively). This result is consistent with previous results reported for GNPs/citrate systems.[107,108]

A similar experiment was conducted above the LCST of the GNPs. A slight increase in the adsorption of BSA was observed for the PEG stabilized GNPs from 0.10 to 0.15 (±0.07) to 0.20−0.35 (±0.07) mg/m^2 and for GNPs/PNIPAAm from 0.44 (±0.14) to 1.3 mg/m^2, consistent with an increase in hydrophobic interactions between the protein and the polymers. BSA has a defined tertiary structure displaying surfaces with both positively and negatively charged domains with a distinct hydrophobic region.[109] In the case of P(OEG-*co*-DEG-A) even above the LCST, the BSA adsorption was still relatively low, suggesting that the hydrophobic interactions are fairly weak. After BSA incubation, the GNP/poly(OEG-A-*co*-DEG-A) nanoparticles could be isolated and redispersed in water. Subsequent DLS and zeta potential measurements reveal that the nanoparticles exhibit similar sizes and surface charges to measurements made prior to the Bradford assay.

The stability of GNPs/poly(OEG-A-*co*-DEG-A) was also studied in 50 vol % of fetal bovine serum (FBS), used as a model system for a biological fluid,[83] below and above the LCST of the grafted polymer layer. The size and zeta potential of these nanoparticles were monitored with time using DLS. Encouragingly, it was found that these nanoparticles stayed perfectly dispersed after 3 days, at temperatures below the LCST.

Two different copolymers, having different LCST behavior (one close to 15 °C, i.e., poly(DEG-A), and one close to 33 °C, i.e., poly(DEG-A-*co*-OEG-A), entry 3 of Table 1), were assembled onto GNPs to form mixed-layer GNP hybrids. These two

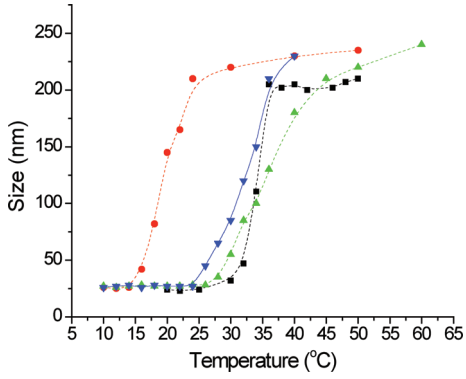

Figure 8. Evolution of size vs temperature for different GNPs: (●) GNPs/poly(DEG-A) [entry 1 of Table 1], (■) GNPs/poly(DEG-A-*co*-OEG-A) [entry 3, Table 1], (▲) GNPs/mixed polymers [poly(OEG-A)/poly(DEG-A-*co*-OEG-A)] = 50/50 wt %], (▼) GNPs/mixed polymers [poly(DEG-A)/poly(DEG-A-*co*-OEG-A)] = 75/25 wt %].

copolymers (of similar molecular weight, both 20 kg/mol) were mixed together in different proportions (25/75, 50/50, and 75/25 wt %) with GNPs yielding hybrid nanoparticles with mixed polymer layer compositions. After purification, the surface layer composition was characterized using XPS, revealing the presence of signals characteristic of C and O bonds, attributable to both OEG-A and DEG-A moieties. Quantification of the polymers grafted onto the gold surface was achieved via elemental composition analysis by XPS. Accordingly, the O/C ratio of poly(DEG-A) and copoly(DEG-A-*co*-OEG-A) (pure nonadsorbed polymer samples) was 44% and 54%, respectively. In the case of hybrid GNPs coated with two different copolymers (50/50 wt %), the ratio O/C was measured to be 48%. Similarly, the O/C ratios were measured to be 46% and 51% for poly(DEG-A)/copoly(DEG-A-*co*-OEG-A) = 75/25 and 25/75 wt %, respectively. The XPS results show that the polymer compositions assembled onto the GNPs correlates strongly with the corresponding compositions of the polymer solutions used for their preparation. All three different stabilizing polymer compositions yielded 30 nm nanoparticles with low polydispersities in solution (determined at 5 °C by DLS).

The effect of temperature on the particle size changes of these GNP dispersions was then assessed using DLS (Figure 8). As the temperature increased slowly up from 5 to 25 °C, no significant change to the characteristic color (i.e., the plasmon absorbance determined by UV−vis spectroscopy) or to the particle size as determined by DLS (a slight decrease) was observed. However as the temperature was further increased to 28−30 °C, slightly lower than the second higher LCST, the properties of the mixed hybrid nanoparticles changed (both color and size). The aggregate sizes increased quickly from 35 to 250 nm, and the solutions underwent a color change to purple, indicating aggregation was occurring. It is also evident from the results presented in Figure 8 that the LCST exhibited by these mixed layered systems is sensitive to the composition of the polymer surface layer. The GNPs coated with 75 wt % of poly(DEG-A) and 25 wt % of poly(OEG-A-*co*-DEG-A) showed a thermoresponsive transition shifted to a lower temperature when compared to the 50/50 mixed polymer hybrid system; i.e., there is a slight decrease in the LCST (about 5 °C) as the amount of poly(DEG-A) on the surface layer increased from 50% to 75%. Moreover, the LCST transition of the hybrid nanoparticles with a mixed polymer layer was broader than those found for the GNPs coated with only one type of polymer. This result can be attributed to the fact that these nanoparticles are stabilized by a distribution of surface layer compositions, displaying slightly different LCSTs.

This outcome demonstrates that the properties of the GNPs in solution are dictated by the bound copolymer with the higher

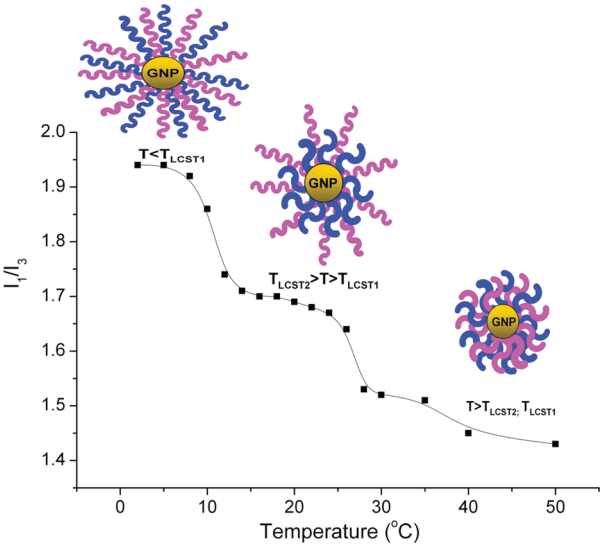

Figure 9. Evolution of I_1/I_3 versus the temperature for GNPs/mixed polymers [poly(DEG-A)/poly(DEG-A-*co*-OEG-A)] = 50/50 wt %].

LCST. We speculate that as the temperature is raised there is a hydrophilic to hydrophobic transition of the copolymer chains with the lower LCST. This transition causes the formation of an internal hydrophobic layer through the collapse of these extended chains to a globular form, but as a whole, the nanoparticles are still stabilized by those copolymer chains with the higher LCST. These chains are still extended from the surface and remain hydrophilic. On further heating the second LCST is reached inducing a hydrophilic−hydrophobic transition. This causes a destabilization of the mixed hybrid nanoparticles in solution, resulting in aggregation.

To confirm this, an experiment was designed to probe the formation of a hydrophobic layer within the mixed hybrid nanoparticles using pyrene.[110] The change in the fluorescent spectrum of pyrene has commonly been used as a hydrophobic probe to evaluate the polarity of the environment surrounding the pyrene molecules. When a hydrophobic domain is present in the water solution, pyrene tends to partition into the hydrophobic domain. On entering these domains, there is a red shift in the emission spectrum, viz. a decrease in the intensity ratio of the first I_1 to the third I_3 vibration bands (Figure S3 in the Supporting Information).[111] GNP/[poly(DEG-A)/poly(OEG-A-*co*-DEG-A) = 50/50 wt %] (1 mg/mL) was mixed with a pyrene solution (10^{-6} mol/L) overnight at 5 °C. The change of I_1/I_3 values versus temperature is shown in Figure 9. Two majors transitions were observed: first (at 8−10 °C), the values dropped from 1.9 to 1.7, followed by a second decrease in the ratio values (from 1.7 to 1.5) around 25−28 °C. This result was found to be completely reversible; if the temperature decreases, these values increase and return to their original values, i.e., 1.9. These LCST values are slightly lower than those determined independently for the two copolymers in aqueous solution; however, it has been shown previously in similar GNP/PNIPAAm hybrid systems that the LCST of the grafted polymer layer is affected by the confinement of the PNIPAAm chains at a surface.[73] The outcome of this experiment demonstrates the systematic formation of a hydrophobic zone in the mixed layer hybrid nanoparticles consistent with two different polymers self-assembled onto the GNP surface. As a control experiment, GNP/[poly(DEG-A)] and GNP/[poly(OEG-A-*co*-DEG-A) were separately analyzed using pyrene. In the case of these two different GNPs, we observed only one change for I_1/I_3 ratio when the temperature was increased. The changes for GNP/[poly(DEG-A)] and GNP/[poly(OEG-A-*co*-DEG-A) were close to 8−10 and 25−28 °C, respectively.

The antifouling properties of these mixed polymer layer GNPs were evaluated as before; below the first LCST, between the two LCSTs, and above the second LCST. A low protein adsorption (~0.10 ± 0.05 mg/m^2) was observed below the first LCST and also between the LCSTs in accord with previous results. The absence significant protein adsorption at the temperature between the two LCSTs confirms the maintenance of a nonfouling layer. A slight increase in BSA adsorption (~0.20 ± 0.10 mg/m^2) was found above the second LCST, in accord with our earlier results.

Clearly, the presence of poly(DEG-A) chains in the layer is affecting the LCST transition of the copoly(DEG-A-*co*-OEG-A) chains. Further experiments to investigate this are underway. Clearly, the composition of the polymer surface layer provides another variable allowing for the precise tuning of the LCST behavior of these hybrid nanoparticles.

Conclusion

In this work, we have demonstrated for the first time the formation of hybrid polymer/GNP nanoparticles using novel PEG-based thermosensitive polymers displaying a broad range of LCST values (from 15 to 90 °C). These hybrid nanoparticles have been shown to have not only tunable thermosensitive behavior but also antifouling/protein resistant surfaces. By judicious choice of the copolymers used in the assembly of these hybrid nanoparticles, it is possible to form hybrid nanoparticles with uniquely nanostructured hydrophilic/hydrophobic polymer surface layers as demonstrated here from the one PEG-based polymer system.

Acknowledgment. T.P.D. acknowledge the Australian Research Council for the award of Discovery Grants and Federation Fellowship.

Supporting Information Available: NMR spectra of copolymers, DLS of "naked" GNPs and GNPs coated polymers, and fluorescence emission spectra of pyrene. This material is available free of charge via the Internet at http://pubs.acs.org.

References and Notes

(1) Chen, P. C.; Mwakwari, S. C.; Oyelere, A. K. *Nanotechnol., Sci. Appl.* **2008**, *1*, 45–66.
(2) Huang, X.; El-Sayed, I. H.; Qian, W.; El-Sayed, M. A. *J. Am. Chem. Soc.* **2006**, *128*, 2115–2120.
(3) Kim, S.; Lim, Y. T.; Soltesz, E. G.; De Grand, A. M.; Lee, J.; Nakayama, A.; Parker, J. A.; Mihaljevic, T.; Laurence, R. G.; Dor, D. M.; Cohn, L. H.; Bawendi, M. G.; Frangioni, J. V. *Nat. Biotechnol.* **2004**, *22*, 93–97.
(4) Krause, W. *Adv. Drug Delivery Rev.* **1999**, *37*, 159–173.
(5) Weissleder, R. *Science* **2006**, *312*, 1168–1171.
(6) De, M.; Ghosh, P. S.; Rotello, V. M. *Adv. Mater.* **2008**, *20*, 4225–4241.
(7) Ghosh, P. S.; Kim, C.-K.; Han, G.; Forbes, N. S.; Rotello, V. M. *ACS Nano* **2008**, *2*, 2213–2218.
(8) Cho, E. C.; Xie, J.; Wurm, P. A.; Xia, Y. *Nano Lett.* **2009**, *9*, 1080–1084.
(9) Javakhishvili, I.; Hvilsted, S. *Biomacromolecules* **2009**, *10*, 74–81.
(10) Aqil, A.; Qiu, H.; Greisch, J.-F.; Jerome, R.; De Pauw, E.; Jerome, C. *Polymer* **2008**, *49*, 1145–1153.
(11) Bergen, J. M.; von Recum, H. A.; Goodman, T. T.; Massey, A. P.; Pun, S. H. *Macromol. Biosci.* **2006**, *6*, 506–516.
(12) Giljohann, D. A.; Seferos, D. S.; Prigodich, A. E.; Patel, P. C.; Mirkin, C. A. *J. Am. Chem. Soc.* **2009**, *130*, 2073–2074.
(13) Zhao, W.; Chiuman, W.; Lam, J. C. F.; McManus, S. A.; Chen, W.; Cui, Y.; Pelton, R.; Brook, M. A.; Li, Y. *J. Am. Chem. Soc.* **2008**, *130*, 3610–3618.
(14) Durocher, S.; Rezaee, A.; Hamm, C.; Rangan, C.; Mittler, S.; Mutus, B. *J. Am. Chem. Soc.* **2009**, *131*, 2475–2477.
(15) Tessier, P. M.; Jinkoji, J.; Cheng, Y.-C.; Prentice, J. L.; Lenhoff, A. M. *J. Am. Chem. Soc.* **2008**, *130*, 3106–3112.

(16) Michalet, X.; Pinaud, F. F.; Bentolila, L. A.; Tsay, J. M.; Doose, S.; Li, J. J.; Sundaresan, G.; Wu, A. M.; Gambhir, S. S.; Weiss, S. *Science* **2005**, *307*, 538–544.
(17) Shan, J.; Tenhu, H. *Chem. Commun.* **2007**, 4580–4598.
(18) Storhoff, J. J.; Lazarides, A. A.; Mucic, R. C.; Mirkin, C. A.; Letsinger, R. L.; Schatz, G. C. *J. Am. Chem. Soc.* **2000**, *122*, 4640–4650.
(19) Daniel, W. L.; Han, M. S.; Lee, J.-S.; Mirkin, C. A. *J. Am. Chem. Soc.*, ASAP.
(20) Park, J. B.; Graciani, J.; Evans, J.; Stacchiola, D.; Ma, S.; Liu, P.; Nambu, A.; Sanz, J. F.; Hrbek, J.; Rodrigue, J. A. *Proc. Natl. Acad. Sci. U.S.A.* **2009**, *106*, 4975–4980.
(21) Della Pina, C.; Falletta, E.; Rossi, M.; Sacco, A. *J. Catal.* **2009**, *263*, 92–97.
(22) Huang, X.; Guo, C.; Zuo, J.; Zheng, N.; Stucky, G. D. *Small* **2009**, *5*, 361–365.
(23) Chen, L.; Hu, J.; Richards, R. *J. Am. Chem. Soc.* **2009**, *131*, 914–915.
(24) Han, J.; Liu, Y.; Guo, R. *J. Am. Chem. Soc.* **2009**, *131*, 2060–2061.
(25) Agasti, S. S.; Chompoosor, A.; You, C.-C.; Ghosh, P.; Kim, C. K.; Rotello, V. M. *J. Am. Chem. Soc.* **2009**, *131*, 5728–5729.
(26) Cheng, Y.; Samia, A. C.; Meyers, J. D.; Panagopoulos, I.; Fei, B.; Burda, C. *J. Am. Chem. Soc.* **2008**, *130*, 10643–10647.
(27) Kim, C. K.; Ghosh, P.; Pagliuca, C.; Zhu, Z.-J.; Menichetti, S.; Rotello, V. M. *J. Am. Chem. Soc.* **2009**, *131*, 1360–1361.
(28) Thomas, M.; Klibanov, A. M. *Proc. Natl. Acad. Sci. U.S.A.* **2003**, *100*, 9138–9143.
(29) Alric, C.; Taleb, J.; Le Duc, G.; Mandon, C.; Billotey, C.; Le Meur-Herland, A.; Brochard, T.; Vocanson, F.; Janier, M.; Perriat, P.; Roux, S.; Tillement, O. *J. Am. Chem. Soc.* **2008**, *130*, 5908–5915.
(30) Alric, C.; Serduc, R.; Mandon, C.; Taleb, J.; Le Duc, G.; Le Meur-Herland, A.; Billotey, C.; Perriat, P.; Roux, S.; Tillement, O. *Gold Bull.* **2008**, *41*, 90–97.
(31) Kim, D.; Park, S.; Lee, J. H.; Jeong, Y. Y.; Jon, S. *J. Am. Chem. Soc.* **2007**, *129*, 7661–7665.
(32) Qian, X.; Peng, X.-H.; Ansari, D. O.; Yin-Goen, Q.; Chen, G. Z.; Shin, D. M.; Yang, L.; Young, A. N.; Wang, M. D.; Nie, S. *Nat. Biotechnol.* **2008**, *26*, 83–90.
(33) Kim, D. J.; Kang, S. M.; Kong, B.; Kim, W.-J.; Paik, H.-j.; Choi, H.; Choi, I. S. *Macromol. Chem. Phys.* **2005**, *206*, 1941–1946.
(34) Dong, H.; Zhu, M.; Yoon, J. A.; Gao, H.; Jin, R.; Matyjaszewski, K. *J. Am. Chem. Soc.* **2008**, *130*, 12852–12853.
(35) Holzinger, D.; Liz-Marzan, L. M.; Kickelbick, G. *J. Nanosci. Nanotechnol.* **2006**, *6*, 445–452.
(36) Li, D.; He, Q.; Cui, Y.; Wang, K.; Zhang, X.; Li, J. *Chem.—Eur. J.* **2007**, *13*, 2224–2229.
(37) Raula, J.; Shan, J.; Nuopponen, M.; Niskanen, A.; Jiang, H.; Kauppinen, E. I.; Tenhu, H. *Langmuir* **2003**, *19*, 3499–3504.
(38) Wei, Q.; Ji, J.; Shen, J. *Macromol. Rapid Commun.* **2008**, *29*, 645–650.
(39) Lowe, A. B.; Sumerlin, B. S.; Donovan, M. S.; McCormick, C. L. *J. Am. Chem. Soc.* **2002**, *124*, 11562–11563.
(40) Zhang, T.; Zheng, Z.; Ding, X.; Peng, Y. *Macromol. Rapid Commun.* **2008**, *29*, 1716–1720.
(41) Shen, Y.; Kuang, M.; Shen, Z.; Nieberle, J.; Duan, H.; Frey, H. *Angew. Chem., Int. Ed.* **2008**, *47*, 2227–2230.
(42) Roth, P. J.; Theato, P. *Chem. Mater.* **2008**, *20*, 1614–1621.
(43) Wang, B.; Li, B.; Zhao, B.; Li, C. Y. *J. Am. Chem. Soc.* **2008**, *130*, 11594–11595.
(44) Sumerlin, B. S.; Lowe, A. B.; Stroud, P. A.; Zhang, P.; Urban, M. W.; McCormick, C. L. *Langmuir* **2003**, *19*, 5559–5562.
(45) McCormick, C. L.; Lowe, A. B. *Acc. Chem. Res.* **2004**, *37*, 312–325.
(46) Li, Y.; Smith, A. E.; Lokitz, B. S.; McCormick, C. L. *Macromolecules* **2007**, *40*, 8524–8526.
(47) Smith, A. E.; Xu, X.; Abell, T. U.; Kirkland, S. E.; Hensarling, R. M.; McCormick, C. L. *Macromolecules* **2009**, *42*, 2958–2964.
(48) Kim, B. J.; Bang, J.; Hawker, C. J.; Chiu, J. J.; Pine, D. J.; Jang, S. G.; Yang, S.-M.; Kramer, E. J. *Langmuir* **2007**, *23*, 12693–12703.
(49) Park, S. C.; Kim, B. J.; Hawker, C. J.; Kramer, E. J.; Bang, J.; Ha, J. S. *Macromolecules* **2007**, *40*, 8119–8124.
(50) Merican, Z.; Schiller, T. L.; Hawker, C. J.; Fredericks, P. M.; Blakey, I. *Langmuir* **2007**, *23*, 10539–10545.
(51) Nuopponen, M.; Tenhu, H. *Langmuir* **2007**, *23*, 5352–5357.
(52) Fustin, C.-A.; Colard, C.; Filali, M.; Guillet, P.; Duwez, A.-S.; Meier, M. A. R.; Schubert, U. S.; Gohy, J.-F. *Langmuir* **2006**, *22*, 6690–6695.
(53) Duwez, A.-S.; Guillet, P.; Colard, C.; Gohy, J.-F.; Fustin, C.-A. *Macromolecules* **2006**, *39*, 2729–2731.
(54) Hotchkiss, J. W.; Lowe, A. B.; Boyes, S. G. *Chem. Mater.* **2007**, *19*, 6–13.
(55) Roth, P. J.; Kessler, D.; Zentel, R.; Theato, P. *Macromolecules* **2008**, *41*, 8316–8319.
(56) Scales, C. W.; Convertine, A. J.; McCormick, C. L. *Biomacromolecules* **2006**, *7*, 1389–1392.
(57) York, A. W.; Scales, C. W.; Huang, F.; McCormick, C. L. *Biomacromolecules* **2007**, *8*, 2337–2341.
(58) Li, M.; De, P.; Gondi, S. R.; Sumerlin, B. S. *J. Polym. Sci., Part A: Polym. Chem.* **2008**, *46*, 5093–5100.
(59) (a) Boyer, C.; Bulmus, V.; Davis, T. P. *Macromol. Rapid Commun.* **2009**, *30*, 493–497. (b) Boyer, C.; Granville, A.; Davis, T. P.; Bulmus, V. *J. Polym. Sci., Part A: Polym. Chem.* **2009**, *47*, 3773–3794. (c) Boyer, C.; Liu, J.; Davis, T. P.; Bulmus, V. *Aust. J. Chem.* **2009**, doi: 10.1071/CH09062.
(60) Peer, D.; Karp, J. M.; Hong, S.; Farokhzad, O. C.; Margalit, R.; Langer, R. *Nat. Nanotechnol.* **2007**, *2*, 751–760.
(61) Kah, J. C. Y.; Wong, K. Y.; Neoh, K. G.; Song, J. H.; Fu, J. W. P.; Mhaisalkar, S.; Olivo, M.; Sheppard, C. J. R. *J. Drug Targeting* **2009**, *17*, 181–193.
(62) Prencipe, G.; Tabakman, S. M.; Welsher, K.; Liu, Z.; Goodwin, A. P.; Zhang, L.; Henry, J.; Dai, H. *J. Am. Chem. Soc.* **2009**, *131*, 4783–4787.
(63) Liu, Y.; Shipton, M. K.; Ryan, J.; Kaufman, E. D.; Franzen, S.; Feldheim, D. L. *Anal. Chem.* **2007**, *79*, 2221–2229.
(64) Chanana, M.; Jahn, S.; Georgieva, R.; Lutz, J.-F.; Baumler, H.; Wang, D. *Chem. Mater.* **2009**, *21*, 1906–1914.
(65) Veronese, F. M.; Harris, J. M. *Adv. Drug Delivery Rev.* **2008**, *60*, 1–2.
(66) Harris, J. M.; Chess, R. B. *Nat. Rev. Drug Discovery* **2003**, *2*, 214–221.
(67) Ryan, S. M.; Mantovani, G.; Wang, X.; Haddleton, D. M.; Brayden, D. J. *Expert Opin. Drug Delivery* **2008**, *5*, 371–383.
(68) Nicolas, J.; San Miguel, V.; Mantovani, G.; Haddleton, D. M. *Chem. Commun.* **2006**, 4697–4699.
(69) Yusa, S.-i.; Fukuda, K.; Yamamoto, T.; Iwasaki, Y.; Watanabe, A.; Akiyoshi, K.; Morishima, Y. *Langmuir* **2007**, *23*, 12842–8.
(70) Ishii, T.; Otsuka, H.; Kataoka, K.; Nagasaki, Y. *Langmuir* **2004**, *20*, 561–564.
(71) Shan, J.; Chen, J.; Nuopponen, M.; Tenhu, H. *Langmuir* **2004**, *20*, 4671–4676.
(72) Shan, J.; Nuopponen, M.; Jiang, H.; Kauppinen, E.; Tenhu, H. *Macromolecules* **2003**, *36*, 4526–4533.
(73) Zhu, M.-Q.; Wang, L.-Q.; Exarhos, G. J.; Li, A. D. Q. *J. Am. Chem. Soc.* **2004**, *126*, 2656–2657.
(74) Boyer, C.; Bulmus, V.; Liu, J.; Davis, T. P.; Stenzel, M. H.; Barner-Kowollik, C. *J. Am. Chem. Soc.* **2007**, *129*, 7145–7154.
(75) Kujawa, P.; Segui, F.; Shaban, S.; Diab, C.; Okada, Y.; Tanaka, F.; Winnik, F. M. *Macromolecules* **2006**, *39*, 341–348.
(76) Van Durme, K.; Rahier, H.; Van Mele, B. *Macromolecules* **2005**, *38*, 10155–10163.
(77) Zhou, Y.; Jiang, K.; Chen, Y.; Liu, S. *J. Polym. Sci., Part A: Polym. Chem.* **2008**, *46*, 6518–6531.
(78) Zheng, P.; Jiang, X.; Zhang, X.; Zhang, W.; Shi, L. *Langmuir* **2006**, *22*, 9393–9396.
(79) Bhattacharjee, R. R.; Chakraborty, M.; Mandal, T. K. *J. Phys. Chem. B* **2006**, *110*, 6768–6775.
(80) Dong, Y.; Ma, Y.; Zhai, T.; Zeng, Y.; Fu, H.; Yao, J. J. *J. Nanosci. Nanotechnol.* **2008**, *8*, 6283–6289.
(81) Jeon, H. J.; Go, D. H.; Choi, S.-y.; Kim, K. M.; Lee, J. Y.; Choo, D. J.; Yoo, H.-O.; Kim, J. M.; Kim, J. *Colloids Surf., A* **2008**, *317*, 496–503.
(82) Tang, T.; Krysmann, M. J.; Hamley, I. W. *Colloids Surf., A* **2008**, *317*, 764–767.
(83) Salmaso, S.; Caliceti, P.; Amendola, V.; Meneghetti, M.; Magnusson, J. P.; Pasparakis, G.; Alexander, C. *J. Mater. Chem.* **2009**, *19*, 1608–1615.
(84) Ernst, O.; Lieske, A.; Hollaender, A.; Lankenau, A.; Duschl, C. *Langmuir* **2008**, *24*, 10259–10264.
(85) Lutz, J.-F.; Akdemir, O.; Hoth, A. *J. Am. Chem. Soc.* **2006**, *128*, 13046–13047.
(86) Lutz, J.-F.; Hoth, A. *Macromolecules* **2006**, *39*, 893–896.
(87) Lutz, J.-F. *J. Polym. Sci., Part A: Polym. Chem.* **2008**, *46*, 3459–3470.
(88) Wischerhoff, E.; Uhlig, K.; Lankenau, A.; Boerner, H. G.; Laschewsky, A.; Duschl, C.; Lutz, J.-F. *Angew. Chem., Int. Ed.* **2008**, *47*, 5666–5668.
(89) Frens, G. *Nat. Phys. Sci.* **1973**, *241*, 20–2.

(90) Bradford, M. M. *Anal. Biochem.* **1976**, *72*, 248–254.
(91) Ghosh, P.; Han, G.; De, M.; Kim, C. K.; Rotello, V. M. *Adv. Drug Delivery Rev.* **2008**, *60*, 1307–1315.
(92) Schneider, G.; Decher, G. *Nano Lett.* **2004**, *4*, 1833–1839.
(93) Schneider, G.; Decher, G. *Langmuir* **2008**, *24*, 1778–1789.
(94) Schneider, G. F.; Decher, G. *Nano Lett.* **2008**, *8*, 3598–3604.
(95) Beamson, G.; Briggs, D. *High Resolution XPS of Organic Polymers*; John Wiley and Sons: Chichester, 1992.
(96) Zhou, C.; Khlestkin, V. K.; Braeken, D.; De Keersmaecker, K.; Laureyn, W.; Engelborghs, Y.; Borghs, G. *Langmuir* **2005**, *21*, 5988–5996.
(97) Zareie, H. M.; Boyer, C.; Bulmus, V.; Nateghi, E.; Davis, T. P. *ACS Nano* **2008**, *2*, 757–765.
(98) Boyer, C.; Bulmus, V.; Priyanto, P.; Teoh, W. Y.; Amal, R.; Davis, T. P. *J. Mater. Chem.* **2009**, *19*, 111–123.
(99) Hirsch, L. R.; Stafford, R. J.; Bankson, J. A.; Sershen, S. R.; Rivera, B.; Price, R. E.; Hazle, J. D.; Halas, N. J.; West, J. L. *Proc. Natl. Acad. Sci. U.S.A.* **2003**, *100*, 13549–13554.
(100) Gao, X.; Yang, L.; Petros, J. A.; Marshall, F. F.; Simons, J. W.; Nie, S. *Curr. Opin. Biotechnol.* **2005**, *16*, 63–72.
(101) Ballou, B.; Lagerholm, B. C.; Ernst, L. A.; Bruchez, M. P.; Waggoner, A. S. *Bioconjugate Chem.* **2004**, *15*, 79–86.
(102) Zheng, M.; Davidson, F.; Huang, X. *J. Am. Chem. Soc.* **2003**, *125*, 7790–7791.
(103) Kohler, N.; Fryxell, G. E.; Zhang, M. *J. Am. Chem. Soc.* **2004**, *126*, 7206–7211.
(104) Herrwerth, S.; Eck, W.; Reinhardt, S.; Grunze, M. *J. Am. Chem. Soc.* **2003**, *125*, 9359–9366.
(105) Lee, H.; Lee, E.; Kim, D. K.; Jang, N. K.; Jeong, Y. Y.; Jon, S. *J. Am. Chem. Soc.* **2006**, *128*, 7383–7389.
(106) Li, L.; Chen, S.; Zheng, J.; Ratner, B. D.; Jiang, S. *J. Phys. Chem. B* **2005**, *109*, 2934–2941.
(107) Brewer, S. H.; Glomm, W. R.; Johnson, M. C.; Knag, M. K.; Franzen, S. *Langmuir* **2005**, *21*, 9303–9307.
(108) Kaufman, E. D.; Belyea, J.; Johnson, M. C.; Nicholson, Z. M.; Ricks, J. L.; Shah, P. K.; Bayless, M.; Pettersson, T.; Feldotoe, Z.; Blomberg, E.; Claesson, P.; Franzen, S. *Langmuir* **2007**, *23*, 6053–6062.
(109) Rezwan, K.; Meier, L. P.; Rezwan, M.; Voeroes, J.; Textor, M.; Gauckler, L. J. *Langmuir* **2004**, *20*, 10055–10061.
(110) Zhang, Y.; Jiang, M.; Zhao, J.; Chen, D. *Eur. Polym. J.* **2007**, *43*, 4905–4915.
(111) Kalyanasundaram, K.; Thomas, J. K. *J. Am. Chem. Soc.* **1977**, *99*, 2039–44.